Molecular basis for the interactions of eIF2β with eIF5, eIF2B, and 5MP1 and their regulation by CK2

Paul A. Wagner,[1] Meimei Song,[1,6] Ralf Ficner,[2] Bernhard Kuhle,[3,4,5,*] and Assen Marintchev[1,7,**]

[1]Department of Pharmacology, Physiology, & Biophysics, Boston University Chobanian & Avedisian School of Medicine, Boston, MA, USA

[2]Department of Molecular Structural Biology, GZMB, University of Göttingen, 37077 Göttingen, Germany

[3]Department of Molecular Biology, University Medical Center Göttingen, 37073 Göttingen, Germany

[4]Research Group Structure and Function of Molecular Machines, Max Planck Institute for Multidisciplinary Sciences, 37077 Göttingen, Germany

[5]Department of Molecular Medicine, The Scripps Research Institute, La Jolla, CA 92037, USA

[6]Present address: Department of Chemistry, University of North Carolina, Chapel Hill, NC, USA

[7]Lead contact

[*]Correspondence: bernhard.kuhle@med.uni-goettingen.de

[**]Correspondence: amarint@bu.edu

Summary

The heterotrimeric GTPase eukaryotic translation initiation factor 2 (eIF2) delivers the initiator Met-tRNAi to the ribosomal translation preinitiation complex. eIF2β has three lysine-rich repeats (K-boxes) in its N-terminal tail, which are important for binding to the GTPase-activating protein (GAP) eIF5, the guanine nucleotide exchange factor (GEF) eIF2B, and the regulator eIF5-mimic protein (5MP). Here, we combine X-ray crystallography with NMR to understand the molecular basis and dynamics of these interactions. The crystal structure of yeast eIF5-CTD in complex with K-box 3 of eIF2β reveals an extended binding site on eIF2β, far beyond the K-box. We show that human eIF5, eIF2Bε, and 5MP1 can all bind to each of the three K-boxes, while reducing each other's affinities. Moreover, all these affinities are increased by CK2 phosphomimetic mutations. Our results reveal how eIF5, eIF2B, and 5MP displace each other from eIF2, and elucidate the role of CK2 in remodeling the translation apparatus.

Introduction

Translation initiation in eukaryotes relies on a complex network of interactions that are continuously reorganized throughout the process. As more information becomes available about the structure of the ribosomal preinitiation complex (PIC) at various points in translation initiation, new questions arise about which interactions occur when, their roles, and regulation. The eukaryotic translation initiation factor 2 (eIF2) is a heterotrimeric GTPase playing a central role in regulation of translation initiation and the integrated stress response (ISR). In its active GTP-bound form, eIF2 binds the initiator Met-tRNAi to form the eIF2-GTP•Met-tRNAi ternary complex (TC). The TC binds to the PIC, either directly or as part of the multifactor complex (MFC), which also includes eIFs 1, 3, and 5. eIF5 is the GTPase-activating protein (GAP) for eIF2. eIF1 serves as a gate-keeper promoting stringency of start codon selection. eIF3 is a 13-mer with multiple roles in translation initiation. Most of it resides on the back, solvent-exposed surface of the 40S ribosomal subunit, while the N-terminus of eIF3c wraps around the 40S and interacts with eIFs 1, 2, and 5. The interactions among the MFC components are not fully understood but it has become clear that they are remodeled upon binding to the PIC, where the MFC components also interact with the 40S ribosomal subunit, the mRNA, and eIF1A. The complex is further continually remodeled at every step of translation initiation, including displacement of eIF1 from the ribosome by the eIF5 N-terminal domain (NTD) upon start codon selection to form the so-called “closed” PIC, arrested at the start codon (reviewed in [1-5]).

Following GTP hydrolysis and the release of eIF2-GDP from the PIC, its reactivation to eIF2-GTP and regeneration of the TC require the guanine nucleotide exchange factor (GEF) eIF2B (a decamer with two copies of five different subunits), which promotes nucleotide exchange and subsequent Met-tRNAi binding to eIF2-GTP. eIF2-GDP is released from the PIC in a stable complex with eIF5, which serves as GDP dissociation inhibitor (GDI). eIF2B has to displace eIF5 before it can promote GDP dissociation from eIF2, thus acting as GDI dissociating

factor (GDF).[6-8] As a result, eIF2 is channeled from the PIC, through eIF5, to eIF2B, and could also be directly transferred from eIF2B back to eIF5 and the MFC at the end of the cycle.[9]

eIF2B is one of the main targets in the regulation of protein synthesis in the cell.[1; 9-11] The activity of eIF2B is regulated by phosphorylation of its substrate eIF2, by binding of nucleotides and cofactors to eIF2B, and by phosphorylation of eIF2B itself by at least two kinases: casein kinase 2 (CK2) stimulates eIF2B activity, while GSK-3β inhibits it. In human, several kinases phosphorylate eIF2α at Serine 51 (S51) in response to various types of stress, including viral infection (PKR), unfolded proteins in the ER (PERK), amino acid starvation (GCN2), and heme deficiency (HRI), in what is collectively known as the Integrated Stress Response (ISR). Phosphorylated eIF2-GDP (eIF2(α-P)-GDP) is a competitive inhibitor of eIF2B. Inhibition of eIF2B activity causes downregulation of global protein synthesis and triggers the ISR by inducing the production of a set of transcription factors and other proteins. The result is the activation of both pro-apoptotic and pro-survival pathways aimed at restoring homeostasis. Since the stressors themselves can cause cell death, either an insufficient or overly aggressive stress response can lead to apoptosis, the latter being the desired outcome in the case of viral infection. Dysregulated ISR is a causative factor in the pathology of a number of neurodegenerative disorders, including Alzheimer's disease. Mutations in all five subunits of eIF2B cause the genetic disease leukoencephalopathy with vanishing white matter (VWM) (reviewed in [4; 9; 11-16]).

The eIF5 mimic protein (5MP), also known as BZW, is a regulator that competes for binding to eIF2 with eIF5, leading to increased stringency of start codon selection, and with eIF2B, leading to modulation of nucleotide exchange on eIF2. 5MP also binds to at least one of the other eIF5 partners, eIF3c. While there are two 5MP isoforms in human, 5MP1/BZW2 and 5MP2/BZW1, most of the studies have been performed on 5MP1.[17-19]

The C-terminal domains (CTD) of eIF5, eIF2Bε, and 5MP are homologous to each other and mediate binding to the intrinsically disordered N-terminal tail of the β subunit of eIF2 (eIF2β-NTT). The interaction is mediated by two acidic/aromatic (AA) boxes in the CTD of eIF5, eIF2Bε, and 5MP and three lysine-rich segments (K-boxes) in eIF2β-NTT (reviewed in [1; 2; 4; 10]). The contact interfaces of eIF5-CTD with eIF1, 1A, and possibly also 3c, appear to overlap with the eIF2β-NTT binding surface; therefore, eIF2β-NTT is presumed to be at least partially displaced from eIF5 within the PIC. [20-22] eIF5 and eIF2Bε also interact with eIF2γ, with eIF2Bε having two binding sites, one in the NTD and another in the CTD.[23-25] Interactions between 5MP and eIF2 outside the eIF2β-NTT have not been reported.

Mammalian eIF5, eIF2Bε, and both 5MP isoforms all have conserved Casein Kinase 2 (CK2) phosphorylation sites in AA-box 2. CK2 phosphorylation of eIF5 leads to stimulation of protein synthesis and cell proliferation.[26] Phosphorylation of eIF2Bε stimulates eIF2B activity.[27] The effect of phosphorylation of 5MP1 or 5MP2 has not been investigated. CK2 has hundreds of substrates, including many eIFs, and regulates protein synthesis in a number of ways.[26; 28-33] CK2, together with mTOR, also phosphorylates eIF2β, which helps recruit the PP1 phosphatase that dephosphorylates eIF2α and suppresses the ISR.[30]

Despite their importance for translation initiation, the molecular basis for the interactions of eIF2β-NTT with eIF5, eIF2Bε and 5MP, their dynamics and regulation remain poorly understood. The presence of three K-boxes suggests that there could be three binding sites in eIF2β, but this possibility has received little attention because of the 1:1 stoichiometry of the relevant complexes. We recently reported that human eIF2β-NTT can bind at least two, and most likely three eIF5-CTD molecules simultaneously,[34] and that phosphomimetic mutations in eIF5-CTD, mimicking CK2 phosphorylation, increase its affinity for eIF2β [34] and eIF1A.[35] Here, we report the crystal structure of the complex of *S. cerevisiae* eIF5-CTD with K-box 3 of eIF2β (eIF2β-K3), which shows an extended binding site on eIF2β that involves segments on both

sides of the actual K-box. We go on to show that this binding mode is conserved with human eIF5, as well as eIF2Bε and 5MP1, and that all three proteins can bind to each of the three K-boxes independently and with similar affinities. Finally, phosphomimetic mutations in all three proteins differentially increase their affinities for each K-box and the intact eIF2β-NTT by up to an order of magnitude. Taken together, our results provide both a structural snapshot of the eIF5-eIF2β interactions as well as a plausible model for the dynamic reorganization and regulation of eIF2β-NTT interactions during the translation initiation cycle.

Results

Crystal structure of eIF2β-NTT bound to eIF5-CTD

To gain insight into the structural basis for eIF2β-eIF5 interactions, we determined the X-ray crystal structure of *S. cerevisiae* eIF5-CTD bound to the eIF2β-NTT. Among different combinations of eIF5 and eIF2β constructs used for initial crystallization trials, only the complex between $eIF5_{201-405}$ and $eIF2\beta_{39-106}$, which contains K2 and K3 and flanking regions, produced well-diffracting single crystals in space group $P3_212$ that were suitable for structure determination.

The final atomic model of the eIF5-eIF2β complex, refined at a resolution of 2.0 Å, contains two copies of $eIF5_{201-405}$ per asymmetric unit (AU), each including residues 201 to 399 and additional vector-encoded residues at the N-terminus ($_{-5}$PGLGS$_{-1}$) (details of data collection and refinement statistics are summarized in **Table 1**). Residues 241-399 of both molecules adopt a compact fold composed of four antiparallel helical repeats (R_I-R_{VI}) that is very similar to the previously reported yeast eIF5-CTD structure (r.m.s.d of 0.8 Å over 133 C_α atoms)[36] (**Figure 1A**). The N-terminal extension (amino acids 201-240), which is part of the linker between the N- and C-terminal domains of full-length eIF5, folds into two additional α-helices (α1 and α2) that

protrude away from the globular CTD and form extensive contacts with symmetry related molecules in the crystal packing. Interestingly, the DWEAR motif, a highly conserved and functionally important region of eIF5, forms the loop between helices α1 and α2 and is inserted into a hydrophobic cleft between α-helices α3, α5, and α8 of another eIF5-CTD molecule in the crystal packing (**Figure S1**). Notably, although this interaction occurs *in trans*, likely as a crystallographic artifact, a similar interaction could be formed *in cis*, which would allow the DWEAR-motif to associate with the CTD (**Figure S1**).

A single eIF2β molecule is bound by only one of the two eIF5-CTDs in the AU. This eIF2β fragment includes residues 66-105 and forms two amphipathic α-helices (αN and αC) flanking an unstructured loop containing K-box 3 (**Figure 1A,B**). Residues 39-65 of eIF2β, including K2, are not resolved and thus appear to be flexible. Helices αN and αC are both well-defined in the electron density and form extensive hydrophobic as well as polar interactions with eIF5. Helix αN (residues 69-79) lies parallel to eIF5 helices α9 and α11 with which it forms a mostly hydrophobic interface (**Figure 1C**). Helix αC (residues 89-103) binds on top of and orthogonal to eIF5 helices α4 and α7, with Phe96 and Leu100 inserted into a hydrophobic pocket on eIF5 and eIF2β-Glu97 forming a salt bridge with eIF5-Lys313 (**Figure 1D**). Between helices αN and αC lies the K3-loop, which is positioned in the immediate vicinity to the negatively charged AA-boxes of eIF5 (area I). Notably, only two of the seven lysine residues, Lys83 and Lys89, form direct interactions with AA-box 1 (**Figure 1E**). The remaining lysine residues of K-box 3 are poorly resolved in the electron density, indicating that they do not participate in stable interactions with eIF5 under the given conditions.

Taken together, the eIF5-bound eIF2β-NTT adopts an elongated conformation, containing secondary, but no tertiary structural features. This allows eIF2β to form an extended interaction interface with eIF5, centered on the K-box and wrapping half around the eIF5-CTD (**Figure 1**). In the following text, 'K-box' will refer to this extended binding site, including the

adjoining segments αN and αC. eIF2β thereby contacts only the periphery of the negatively charged area I of eIF5, with αN and αC lying between the negatively charged areas I and III and the positively charged area II (**Figure 1B**). Most of area I remains solvent-exposed in the complex, including the highly negatively charged C-terminus (residues 393-405), Glu358, and Glu359, which are critical for high affinity binding of eIF2β-NTT [37; 38].

eIF5-CTD, eIF2Bε-CTD, and 5MP1-CTD form similar complexes with each of the three eIF2β-NTT K-boxes.

Multiple-sequence alignments of eIF2β-NTT sequences shows that the segments surrounding the K-boxes are conserved both among species and among the three K-boxes, enriched in acidic and hydrophobic amino acids (**Fig. 2A**). If the binding sites centered around K1 and K2 are similar in size to that observed with K3 in the crystal structure (**Fig. 1**), then in *S. cerevisiae* eIF2β-NTT, the three binding sites are immediately adjacent to each other, with helix αN of one binding site starting where helix αC of the previous binding site ends (**Fig. 2A**). In contrast, in human eIF2β-NTT, there are about 30 amino acids between the predicted K1 and K2 binding site, and about 10 amino acids between K2 and K3 (**Fig. 2A**). The spacer between the end of helix αC after K3 and the eIF2γ-binding helix appears to be about 20 amino acids in both human and *S. cerevisiae* eIF2β-NTT.

We used NMR CSP assay to compare the contact surfaces of eIF5-CTD for each of the three K-boxes and the complete eIF2β-NTT (constructs used in this work are shown in **Fig. 2B**). Comparison of the ^{15}N-TROSY-HSQC spectra of free ^{15}N/^{2}H-labeled eIF5-CTD and of eIF5-CTD in complex with unlabeled individual K-boxes and eIF2β-NTT shows that the vast majority of the peaks affected by binding are the same in all four complexes, with even the magnitude of the peak movement being similar as well (**Fig. 2C**). Mapping the affected amino acids on the surface of eIF5-CTD (**Fig. 2D**) shows that the contact interface is similar to that observed in the

crystal structure of the yeast eIF5-CTD•eIF2β-K3 complex (**Fig. 1**), and also extends into the intrinsically disordered eIF5 C-terminal tail (**Fig. 2D**). Note that in **Fig. 2D**, the position of eIF5-CTT is from the crystal structure of human eIF5-CTD (2iu1.pdb,[39]). However, we have previously shown that the CTT is intrinsically disordered and remains disordered while contacting eIF2β.[34] Accordingly, the corresponding region of *S. cerevisiae* eIF5 (residues 400-405), which is not resolved in the crystal structure (**Fig. 1**), could also be involved in dynamic interactions with eIF2β. Consistent with the crystal structure of the *S. cerevisiae* complex, mutating hydrophobic residues N-terminal from K1, corresponding to helix αN, or deleting a segment C-terminal from K3, corresponding to the C-terminal portion of helix αC, weakens binding to eIF5-CTD by at least an order of magnitude, based on the concentration of the labeled eIF5-CTD (50 μM) and the unlabeled mutant K-boxes (25 μM) (**Fig. S2A** and **B**, respectively). Therefore, the human eIF5-CTD complexes with all K-boxes are very similar and likely similar to the structure of the complex of *S. cerevisiae* eIF5-CTD with eIF2β-K3 (**Fig. 1**).

NMR backbone resonance assignments are not available for eIF2Bε-CTD and 5MP1-CTD, meaning that we do not know which peak in the TROSY-HSQC spectra corresponds to which residue in the protein. However, as with eIF5-CTD, the vast majority of the peaks in the eIF2Bε-CTD and 5MP1-CTD spectra, affected by binding of the three individual K-boxes or the entire eIF2β-NTT, are the same in all four complexes, with even the magnitude of the peaks being similar (**Fig. S3**). Therefore, as for eIF5-CTD, the same surfaces of eIF2Bε-CTD and 5MP1-CTD are affected in all four complexes. Thus, all three proteins form similar complexes with all three K-boxes, both in isolation and when part of the three-K-box eIF2β-NTT (**Fig. 2** and **Fig. S3**).

eIF5-CTD, eIF2Bε-CTD, and 5MP1-CTD have distinct binding affinities for eIF2β-NTT and individual K-boxes.

We used NMR CSP assay titrations to obtain the K_Ds of eIF5-CTD, eIF2Bε-CTD, and 5MP1-CTD binding to each of the three K-boxes and the intact eIF2β-NTT (**Fig. 3** and **Table 2**). Binding is in fast to intermediate exchange on the NMR time scale, depending on the degree of change in peak position (**Fig. 3A**). Peaks that move by > 100 Hz (0.2 ppm for ^{1}H) undergo exchange broadening; therefore, under the experimental conditions (150 mM KCl and 25℃), k_{off} is in the order of 100 s^{-1} (reviewed in [40]). The effect of eIF2β-NTT binding is the weighted average of the binding of the three individual K-boxes. The presence of one average peak for the bound state indicates that each molecule of the labeled protein constantly samples all three K-boxes on the NMR time scale (**Fig. 2C** and **S3**). Because eIF2β-NTT has three non-equivalent binding sites, obtaining all three K_Ds reliably is only possible if they differ by at least 5-fold (and the three binding sites are occupied mostly consecutively). However, at least the average K_D (assuming three binding sites with identical affinities) can always be obtained.

We found that eIF5-CTD binds to all three eIF2β-NTT K-boxes with similar affinities (**Fig. 3B**). In contrast, eIF2Bε-CTD has greater affinity for K2 and K1 than for K3 (**Fig. 3C**). As a result, eIF5-CTD has a much higher affinity for K3 than eIF2Bε-CTD, whereas their affinities for K1 and K2 are comparable (compare **Fig. 3B** and **C**). 5MP1-CTD binds with similar affinities to all three eIF2β-NTT K-boxes (**Fig. 3D**), a few-fold weaker than eIF5-CTD and eIF2Bε-CTD (**Fig. 3, Table 2**). The relative affinities for a given K-box ranged from similar (eIF5-CTD and eIF2Bε-CTD for K2) to different by an order of magnitude (eIF5-CTD and 5MP1-CTD for K3). Overall, K3 shows clear preference for eIF5-CTD, whereas the K_Ds of the proteins for K1 and 2 are much closer (**Fig. 3**, **Table 2**).

Surprisingly, the affinities for eIF2β-NTT are lower than expected from the K_Ds for the individual K-boxes. For eIF2Bε-CTD and 5MP1, the average K_D, calculated assuming three binding sites with equal affinities, is not only higher than the average of the K_Ds for the three individual K-boxes, but 2-fold higher than the highest K_D. For eIF5-CTD, this difference is even

greater: the average K_D for eIF2β-NTT is 6-fold higher than the highest individual K_D, that for K2 (**Fig. 3**, **Table 2**). As a result, the overall affinities of all three proteins for eIF2β-NTT end up being similar to each other (**Table 2**). As described above, the peak positions in the presence of eIF2β-NTT are the weighted average of their positions in the presence of the three individual K-boxes. This weighted average appears similar to the relative affinities for the three K-boxes measured in isolation, both when eIF2β-NTT is in excess and there is on average only one occupied K-box (**Fig. 2C** and **S3**), and when its binding partner is in excess, and all three sites are partially occupied (*data not shown*). Therefore, it appears that binding to all three K-boxes is weaker when part of the eIF2β-NTT.

5MP1 and 5MP1-CTD are partially dimeric at physiological concentrations.

SEC shows that 5MP1 and 5MP1-CTD dimerize, whereas the MA3 domain is monomeric (**Fig. S4A**). The mobility of 5MP1-CTD varies with concentration over the entire range tested, from 500 nM to 500 μM (**Fig. S4B**). Changes in MW_{app} are still observed with concentrations below 1 μM, but the differences become smaller, indicating that below 1 μM, 5MP1 is predominantly, but not completely monomeric. Therefore, the K_D of dimerization is likely near 10 μM, but an accurate K_D cannot be extracted from SEC experiments, because diffusion causes gradual dilution of the sample during the run.

Varying the 5MP1-CTD concentration in the NMR samples causes CSPs in a number of peaks (**Fig. S4C**) because the equilibrium between dimers and monomers shifts with changing its concentration. The peaks that move with changing the protein concentration correspond to amino acids affected by dimerization (whose environment is different between the monomer and dimer). Increasing the salt concentration only modestly weakens dimerization, indicating a major hydrophobic component (*data not shown*).

The 5MP1 dimerization interface overlaps with the eIF2β-NTT contact surface.

Intriguingly, comparison of the 5MP1-CTD NMR spectra shows that all peaks affected by dimerization are also affected by eIF2β-NTT binding (**Fig. S4C**). Some of these peaks show large CSP effects, indicating that the corresponding amino acids are at the interface with eIF2β-NTT. Other peaks move in the complex with eIF2β-NTT in the same direction as when lowering the 5MP1-CTD concentration. While this could be due to a coincidence, where the environment around these amino acids is similar in the monomer and in the complex with eIF2β-NTT, the simplest explanation is that these are not part of the eIF2β-NTT contact surface and binding to eIF2β-NTT disrupts the dimer.

Phosphomimetic mutations in eIF5-CTD, eIF2Bε-CTD, and 5MP1-CTD differentially enhance binding to eIF2β-NTT and individual K-boxes.

As described in the Introduction, eIF5-CTD, eIF2Bε-CTD, and 5MP1-CTD all have conserved CK2 phosphorylation sites in their AA-box 2, which is important for eIF2β binding. While phosphorylation of eIF5-CTD [26] and eIF2Bε-CTD [27] by CK2, and its biological effects have been studied *in vitro*, phosphorylation of the 5MPs has only been observed in high-throughput studies (see e.g. [41; 42]). Therefore, we first confirmed that 5MP1-CTD is readily phosphorylated by CK2 *in vitro* (*data not shown*). Phosphomimetic mutations mimicking CK2 phosphorylation in all three proteins increased their affinities for eIF2β-NTT and the individual K-boxes (**Fig. 4, Table 2**). However, the degree of increase varied significantly, from 50% (5MP1-CTD-EE with K3) to an order of magnitude (eIF5-CTD-EE with K2). The increase in average affinity for eIF2β-NTT also ranged from 50% (5MP1-CTD-EE) to an order of magnitude (eIF5-CTD-EE) (**Table 2**). The overall pattern observed was that the phosphomimetic mutations in eIF5-CTD increased its

affinity to a greater extent than those in eIF2Bε-CTD or 5MP1-CTD. Among the different eIF2β constructs tested, the phosphomimetic mutations increased the affinities for K2 the most (at least three-fold or greater change in K_D). Notably, the affinity of eIF2Bε-CTD-EE for K123 was equal to its affinity for K3, while still being much weaker than the average of its affinities for the three individual K-boxes. The phosphomimetic mutations changed the relative affinities among the three proteins for a given K-box by up to three-fold, in favor of eIF5-CTD (**Table 2**). Therefore, phosphorylation by CK2 modulates the relative affinities of the individual proteins for eIF2β-NTT, in addition to increasing all their affinities.

Discussion

Structure of the eIF2β-K3•eIF5-CTD complex

In the crystal structure of the *S. cerevisiae* eIF2β-K3•eIF5-CTD complex (**Fig. 1**), eIF2β-K3 and the adjoining sequences wrap half-around eIF5-CTD and fold upon binding, forming two helices, αN and αC. The K-box itself forms the loop between the two helices and the N-terminal portion of αC. The eIF5-bound eIF2β-K3 adopts an elongated conformation, with no tertiary structural features (**Figure 1**). Our NMR data (**Fig. 2** and **S3**) show that each of the three K-boxes in human eIF2β forms similar complexes with eIF5-CTD, eIF2Bε-CTD, and 5MP1, suggesting a common interface similar to that observed in the *S. cerevisiae* eIF2β-K3•eIF5-CTD complex (**Fig. 1**). In the crystal structure, most of negatively charged area I in eIF5-CTD, including the highly negatively charged C-terminus, remains available for possible dynamic interactions with K1, K2, and/or K3. The NMR spectra show that the entire negatively charged area I does indeed contact the K-box eIF5-CTD is bound to (**Fig. 2**). Unfortunately, we were

unable to obtain evidence for or against a second K-box simultaneously contacting this surface in eIF5-CTD.

Sequence analysis indicates that in *S. cerevisiae*, almost the entire eIF2β-NTT is made up of three adjacent extended binding sites, except the last 20 or so residues, which form a spacer between the end of K3 helix αC and the eIF2γ-binding helix (**Fig. 2A**). Notably, helix αC ends just above the first of the four antiparallel helical repeats (R_I) of eIF5-CTD (**Fig. 1**), thus supporting the role of eIF2β-NTT in recruiting and positioning the eIF5-CTD and the preceding DWEAR motif relative to the eIF2αβγ complex. In human, the eIF2β-NTT is longer, and the three extended binding sites are not adjacent (**Fig. 2A**). It is not clear whether this difference has any functional significance. However, it should be pointed out that in human, eIF2β-NTT has additional regulatory roles: it has a binding site for raptor (and thus MTORC1) and is phosphorylated by both MTORC1 and CK2, which promotes binding of NCK1, an adaptor of the PP1 phosphatase, leading to eIF2α dephosphorylation and blunting of the ISR. [30]

Stoichiometry of binding to eIF2β-NTT

As described in the Introduction, the GAP eIF5, the GEF eIF2B, and the translational regulators 5MP1 and 2 compete for binding to the GTPase eIF2. eIF5 and eIF2B hand off eIF2 between each other as part of the translation initiation process, while the 5MPs compete with eIF5 and eIF2B for binding to eIF2. [17-19] Binding of the homologous CTDs of eIF5, eIF2Bε, and 5MP to eIF2β-NTT serves to anchor the proteins to eIF2; eIF5 and eIF2B also contact eIF2γ.[23-25] Traditionally, eIF2β-NTT has been considered as one binding site. Accordingly, binding to eIF2β is typically analyzed assuming a binary complex with one binding site, leading to the notion that eIF2 forms 1:1 complexes with eIF5 and eIF2Bε.[4; 43; 44] However, accumulating direct and indirect evidence has indicated that eIF2β-NTT has three binding sites, instead. A complex, where eIF2 was simultaneously bound to eIF2B and eIF5 was reported in *S. cerevisiae*.[8] More

recently, binding of human 5MP1-CTD to an eIF2β-K23 fragment (aa. 53-135) yielded a 2:1 ratio. However, binding of full-length 5MP1 to the same eIF2β fragment appeared to show a 1:1 stoichiometry, leading the authors to conclude that the N-terminal MA3 domain of 5MP1 ensures 1:1 binding.[44] eIF5-CTD binding to the same eIF2β-K23 fragment (aa. 53-135) showed a 1:1 stoichiometry.[21] These results are difficult to interpret in the context of the crystal structure of the *S. cerevisiae* eIF5•eIF2β-K3 complex (**Fig. 1**), because the human eIF2β 53-135 fragment is missing part of the residues corresponding to helix αC in the yeast complex (**Fig. 2A**), which could weaken binding to K3 (**Figure S2B**). Notably, although the yeast eIF2β construct used for structure determination (residues 39-106) included both K2 and K3, K2 does not contact eIF5, leaving it available for further interactions.

What is the stoichiometry *in vivo*? And why are these multiple binding sites present in eIF2β-NTT? Extensive proteomics data in paxdb.org[45] shows that in human cells, the combined number of eIF5, eIF2B, 5MP1, and 5MP2 molecules is greater than that of eIF2, typically 1.5-fold, and up to twice as large.[45] The same is true in *S. cerevisiae*, which does not have a 5MP homolog, but the combined concentrations of eIF5 and eIF2B are greater than that of eIF2, again about 1.5-fold.[45] Therefore, *in vivo*, the majority of eIF2β-NTT would typically be bound to one or two of these proteins. As to why, the answer must be regulation. Specifically, formation of a transient complex, where two proteins are bound simultaneously to eIF2β-NTT, likely allows fast displacement of one protein bound to the trimeric eIF2 by another. For example, this could be involved in eIF2B displacing eIF5 from eIF2-GDP in order to initiate nucleotide exchange on eIF2.[6-8] Such speeding up of the interchange between eIF2-bound proteins would be more efficient if simultaneous binding of two proteins to eIF2β-NTT weakens their affinities, as discussed below.

Here, we report that eIF5-CTD, eIF2Bε-CTD, and 5MP1-CTD form very similar complexes with each of the three K-boxes, whether in isolation or within the intact eIF2β-NTT

(**Fig. 2**, **S3**), akin to the *S. cerevisiae* eIF5•eIF2β-K3 complex (**Fig. 1**). The affinities of individual proteins to different K-boxes vary by up to an order of magnitude, indicating defined preferences of proteins for one K-box over another, and preferences of K-boxes for one protein over another, respectively. At the same time, most of the individual affinities are high enough and similar enough to be physiologically relevant (**Table 2**). Therefore, all three proteins can form similar complexes with each of the K-boxes individually. In *S. cerevisiae*, GCN2 phosphorylates eIF2β on Ser80, which increases its affinity for eIF5, but has no effect on its affinity for eIF2Bε.[46] This finding provides indirect evidence that in *S. cerevisiae*, eIF5 may prefer K3, while eIF2Bε could bind preferentially to K1 or 2, which is consistent with the binding affinities we measured for the human proteins (**Table 2**).

The average affinity for the intact eIF2β-NTT is weaker than the average of the affinities for the three individual K-boxes, in most cases even weaker than the weakest affinity for an individual K-box (**Table 2**), indicating that the three K-boxes interfere with each other's binding, especially to eIF5. As discussed above, in *S. cerevisiae* eIF2β-NTT, there may not be spacers between the binding sites (**Fig. 2A**), fully consistent with direct steric interference between proteins bound to adjacent K-boxes. However, in human eIF2β-NTT, the K-boxes are farther apart (**Fig. 2A**); thus, steric interference was not expected *a priori*. Another possible (and not mutually exclusive) explanation is that a protein bound to one K-box and the surrounding segments, could transiently contact another K-box. Such contacts could interfere with a second protein binding to the second K-box. Consistent with this idea, there are negatively charged surfaces in eIF5-CTD that remain unoccupied in the crystal structure of the complex with K3 (**Fig. 1**) but display NMR CSP effects (**Fig. 2**), indicating that they contact the K-box at least dynamically. It is conceivable that a second K-box could compete for these transient interactions with the "main" K-box. In view of the greater proximity of the individual K-boxes in *S. cerevisiae*

(**Fig. 2A**), it is possible that the degree of interference between proteins bound simultaneously to adjacent K-boxes could be even greater than observed here for the human proteins.

How is eIF2 handed off between eIF5 and eIF2B?

eIF2-GDP leaves the 48S PIC in complex with eIF5, at least in *S. cerevisiae*, [6-8] and likely also in mammals. The process of recycling of eIF2-GDP to the eIF2-GTP-Met-tRNAi TC is in the order of seconds.[47] The K_D of the eIF5•eIF2-GDP complex is in the 10s of nM range and the protein concentrations are in the 100s of nM to μM range (reviewed in [9]). Therefore, the equilibrium is shifted toward complex formation; and the dissociation rate may also be too slow to allow fast enough spontaneous dissociation of eIF2-GDP from eIF5. Instead, eIF2B needs to displace eIF5 from eIF2-GDP before it can promote nucleotide exchange; [6-8] and at the end of the process, eIF5 may need to displace eIF2B from the TC.[1; 9] However, it remains unknown how eIF2B speeds up eIF5 dissociation from eIF2, and *vice versa*. The results presented here offer possible molecular mechanisms for this displacement.

- Both eIF2B and eIF5 contact eIF2 at two or more separate surfaces, yielding a stable interaction with an overall K_D in the 1-20 nM range (reviewed in [9]). However, binding to the eIF2β-NTT alone has a K_D from hundreds of nM to μM (**Table 2** and refs. [7; 21; 34; 44]), with a dissociation rate in the range of milliseconds (see e.g., **Fig. 2C**). This means that in the eIF5•eIF2-GDP complex, eIF5-CTD dissociates and re-binds to eIF2β-NTT tens of times per second, without the eIF5•eIF2 complex falling apart, unless the other contacts are also simultaneously broken. The same should also be the case with the contacts involving eIF2γ. While the proteins can transiently dissociate from each individual binding site on eIF2, e.g., eIF5-CTD dissociation from eIF2β-NTT, the remaining interaction(s) not only preserve the integrity of the complex, but also increase the local concentration of eIF5-CTD. eIF2Bε-CTD binding to a different K-box on eIF2β, simultaneously with eIF5-CTD,

would increase the effective concentration of eIF2B for its other binding sites on eIF2. This would increase the probability of eIF2B binding to eIF2γ when eIF5 transiently vacates its binding site there, which in turn would accelerate eIF5 dissociation from eIF2 (**Fig. 5**).

- Our data indicates that a protein bound to one K-box weakens the affinity of a protein binding to another K-box (**Table 2**), also leading to accelerated dissociation (illustrated with red T-shaped lines in the model in **Fig. 5**).
- Finally, eIF5-CTD and eIF2Bε-CTD binding to each other's preferred binding site on eIF2β would have a direct effect in reducing re-binding to eIF2β.

All of this applies equally to eIF5 displacing eIF2B, presumably from the TC, if TC dissociation from eIF2B is too slow and/or the equilibrium is shifted too far toward the eIF2B•TC complex.[9] In the eIF2B•TC complex, eIF2α-NTD would likely contact the Met-tRNAi, and not eIF2B, which would presumably weaken the eIF2B – eIF2 interaction, but not the eIF5 – eIF2 interaction. As a result, by simultaneously binding to eIF2, eIF5 and eIF2B weaken each other's affinities, leading to accelerated dissociation rates.

Intriguingly, it has been known for decades that eIF2B associates with ribosomes and can be purified from the ribosomal fraction of cell lysates, in complex with eIF2 (see e.g., [47-49]). eIF2B has no known roles within the ribosomal PIC and is not known to bind to any other PIC components; thus, the association of eIF2B with ribosomes has received little attention. However, the ability of eIF2B and eIF5 to bind to eIF2 simultaneously suggests the possibility that eIF2B may be able to displace eIF5 from eIF2 before, in addition to after, eIF2-GDP is released from the PIC.

Regulation of translation initiation by the 5MPs

As described in the Introduction, 5MPs compete with eIF5 and eIF2B for binding to eIF2. In addition to direct competition with eIF5 and eIF2B, our results show that affinity can be modulated by binding simultaneously, as described above for the competition between eIF5 and eIF2B. In view of the observation that 5MP1 has lower affinity, especially compared to eIF5, simultaneous binding would allow 5MP1 to modulate the eIF2 affinity for eIF5 and eIF2B without the need to win a direct competition.

The finding that 5MP1 dimerizes, and that the dimerization interface overlaps with the eIF2β-NTT binding surface, offers yet another avenue for regulation. If eIF2β-NTT binding interferes with 5MP1 dimerization, then dimerization would weaken eIF2β-NTT binding. It will be interesting to test whether binding of other proteins (perhaps eIF3c?[18]) to 5MP1 also affects dimerization. If binding of multiple proteins competes with dimerization, they could bind to 5MP1 cooperatively, because binding of the first protein will have already disrupted the dimer.

Regulation of translation by CK2

CK2 is an essential constitutively active kinase with hundreds of substrates. It is important for both cell proliferation and differentiation and its levels vary among cell types and conditions. CK2 phosphorylates multiple translation factors and has wide-ranging effects on protein synthesis.[26; 28-33] While a CK2 knockout cell line had been reported,[28] it was later found to have residual CK2 activity, about one tenth of that in WT cells.[51]

The homologous eIF5-CTD, eIF2Bε-CTD, 5MP1-CTD, and 5MP2-CTD have conserved consensus CK2 phosphorylation sites within AA-box 2[41; 42]. CK2 phosphorylates at least eIF5-CTD,[26] eIF2Bε-CTD,[27], and 5MP1-CTD (data not shown). AA-box 2 is important for binding to eIF2β-NTT.[43] We recently showed that a phosphomimetic mutation in eIF5-CTD, mimicking CK2

phosphorylation increases its affinity for both eIF2β-NTT and eIF1A, which compete for eIF5 binding.[34; 35] Here, we show that CK2 phosphomimetic mutations stimulate the affinities of eIF5-CTD, eIF2Bε-CTD, and 5MP1-CTD for both the intact eIF2β-NTT and for every individual K-box, with the degree of stimulation ranging from less than two-fold to an order of magnitude (**Table 2**). Thus, CK2 not only shifts the equilibrium among multiple competing interactions, but also stabilizes all of them, potentially stabilizing the PIC and making the entire process more efficient. The stringency of start codon selection is controlled by the interplay among eIF1, eIF5, and the 5MPs.[50; 55; 56] Therefore, translation initiation at suboptimal start codons will likely also be modulated by eIF5 and 5MP phosphorylation.

In addition to eIF5, eIF2Bε, 5MP1, and 5MP2, CK2 also phosphorylates their binding partner, eIF2β. It is not yet known whether the phosphorylation affects binding to eIF5, eIF2Bε, and the 5MPs, but it has been reported to promote the recruitment of NCK1, adapter for the PP1 phosphatase. The resulting dephosphorylation of eIF2α blunts the induction of ISR.[30] Lower CK2 activity could also lead to dephosphorylation of eIF2β-NTT, decrease in NCK1 binding, and thus promote ISR. However, the actual outcome is difficult to predict because mTORC1, which also phosphorylates eIF2β-NTT, was found to be active during chronic stress.[52]

Another interesting example of translation regulation by CK2 is the cap-binding function of eIF3d. Under homeostatic conditions, eIF3d is phosphorylated by CK2, which suppresses its cap-binding ability. However, during chronic stress, eIF3d becomes increasingly dephosphorylated, leading to translation of multiple mRNAs via eIF3d/cap-dependent, but eIF4E-independent mechanisms.[52-54] Dephosphorylation of eIF5 under chronic stress would lower its affinities for eIF2 and eIF1A, which could lead to destabilization of the PIC as a whole, at the same time as the eIF3d cap-binding activity is derepressed. Notably, this drop in binding affinity among eIFs due to loss of phosphorylation by CK2, and the resulting possible destabilization of the PICs would coincide with a drop in overall protein synthesis, and thus

cellular concentrations of ribosomes and eIFs, which are proportional to the rates of protein synthesis.[57] This raises the possibility for the formation of PICs with alternative properties under these conditions. In view of all these considerations, it would be very intriguing to elucidate how the translation apparatus operates under chronic stress.

The results presented here indicate that the differences in translation under various conditions, e.g., under chronic stress vs. actively dividing cells, may not be as simple as having different numbers of ribosomes and translation factors, but likely include kinetic and possibly even structural differences in the translational apparatus. This reinforces the need to always be mindful of the posttranslational modifications present under the specific conditions studied, especially when performing quantitative analysis or modeling.

Materials and Methods

Protein expression and purification

All *S. cerevisiae* constructs were expressed in *E. coli* BL21(DE3) Rosetta II cells (Novagene). Cells transformed with the respective plasmid were grown in 2xYT (containing the appropriate antibiotics) at 37 °C with shaking at 220 rpm until they reached an OD_{600} of ~0.8 and were subsequently transferred to 16 °C. After allowing the cultures to cool down for 20 min, the expression was induced by the addition of isopropyl-β-D-thiogalactopyranosid (IPTG) to a final concentration of 0.5 mM. The cells were harvested after 16 hours at 16 °C. All human constructs were expressed in *E. coli* BL21(DE3) (Novagene), grown in LB at 37 °C. Expression was induced at 20 °C O/N with 1 mM IPTG. $^{15}N/^{2}H$-labeled proteins were expressed in minimal medium in $^{2}H_2O$, with ^{15}N-NH_4Cl as the only nitrogen source, using the same procedure. $^{15}N^{2}H$-labeled eIF2Bε-CTD-EE had poor solubility. Therefore, ^{15}N-labeled eIF2Bε-CTD-EE was used, instead, expressed in minimal medium with ^{15}N-NH_4Cl as the only nitrogen source, using the same procedure.

All yeast eIF2β variants were cloned into the pGEX-6P1 vector and expressed as N-terminal GST-fusion proteins. Cells were resuspended in lysis buffer (500 mM NaCl, 20 mM HEPES (pH 7.5), 5% glycerol, 0.1 mM EDTA, 4 mM β-mercaptoethanol (BME)) supplied with a mixture of protease inhibitors including aprotinin, leupeptin, pepstatin (ALP), and PMSF. The cells were lysed in a microfluidizer (Microfluidics, USA) and cell debris was removed by centrifugation for 30 min at 30,000xg. After centrifugation, the supernatant was loaded onto a GSTrap column (GE Healthcare) equilibrated in lysis buffer. The column was washed with 2 column volumes of lysis buffer and bound fusion protein was eluted lysis buffer containing 30 mM of reduced glutathione. Fractions containing target protein were pooled and incubated over night at 4°C with PreScission protease (GE Healthcare) at a ratio of 1:100 (w/w) of protease to fusion protein to remove the GST-tag. After a desalting step in 200 mM NaCl, 20 mM HEPES pH 7.5, 5% glycerol, 4 mM BME, the cleaved GST, PreScission protease, and uncleaved protein were removed by a second GSH-Sepharose step. The flow-through containing the cleaved eIF2β was pooled and applied to a Superdex S200 column (GE Healthcare) equilibrated in a buffer containing 150 mM KCl, 10 mM HEPES (pH 7.5), 5% glycerol, 2 mM DTT.

All yeast eIF5-CTD constructs were cloned into pGEX-6P1 for expression as N-terminal GST-fusions and purified similar to eIF2β with minor modifications. Following lysis and sample application in lysis buffer, the GSTrap column was equilibrated in low salt buffer (100 mM NaCl, 10 mM HEPES pH 8, 5% glycerol, 4 mM BME), followed by elution in low salt buffer containing 30 mM reduced glutathione. After removal of the GST-tag by PreScission protease treatment, the protein was loaded onto a Source 30Q column (GE Healthcare) equilibrated in low salt buffer. Bound eIF5-CTD was eluted with a linear gradient into high salt buffer (1 M NaCl, 10 mM HEPES pH 7.5, 5% glycerol, 4 mM BME). Fractions containing the target protein were pooled and loaded onto a Superdex S75 column (GE Healthcare) equilibrated in buffer containing 150

mM KCl, 10 mM HEPES pH 7.5, 5% glycerol, 2 mM DTT. Fractions containing pure target protein were pooled, concentrated, flash-frozen in liquid nitrogen, and stored at -80 °C.

Expression and purification of recombinant His_6-tagged human eIF2β-NTT (residues 1-191)[21], eIF5-CTD_{-CTT} (residues 232-431) and its phosphomimetic mutant[34] was as described previously. All other human constructs were cloned in pET21a with an N-terminal GB1 tag, a His_6-tag and a TEV protease cleavage site. Phosphomimetic point mutations were generated by site-directed mutagenesis. The proteins were purified on a TALON Cell-Thru His-tag affinity column (Clontech) in a buffer containing 10 mM Na Phosphate (pH 7.0), 300 mM KCl, 7 mM BME, and 0.1 mM AEBSF, followed by ion exchange chromatography on a Uno Q column, using a 100 mM to 1 M NaCl gradient. Where necessary, the GB1 tag was cleaved using TEV protease. Ion exchange chromatography on a Uno Q column was used to remove the GB1 tag. Proteins were exchanged into buffer containing 10 mM Na Phosphate (pH 7.0), 150 mM KCl, 1 mM EDTA, 0.02% NaN_3, 1 mM DTT, and 0.1 mM AEBSF.

Reconstitution, crystallization, and structure determination of the eIF5-eIF2β complex

The individual yeast proteins, eIF2β_{39-106} and eIF5$_{201-405}$, were purified as described above. The complex was reconstituted in binding buffer (150 mM KCl, 10 mM HEPES pH 7.5, 5% glycerol, 2 mM DTT) by mixing eIF5$_{201-405}$ with a 1.5-fold molar excess of eIF2β_{39-106}. After incubation for 30 min at 20 °C, the complex was separated from excess eIF2β_{39-106} by size exclusion chromatography on a Superdex S75 equilibrated in binding buffer. The purified complex was concentrated to ~20 mg/ml and directly used for crystallization trials.

Crystallization trials were performed using the sitting drop vapor diffusion method. Initial crystals of the eIF5$_{201-405}$/eIF2β_{39-106} complex grew within one day at 20 °C in a condition containing 0.4 M $(NH_4)_2SO_4$ and 0.05 M Li_2SO_4. After optimization, high-quality crystals that were used for structure determination were obtained with 12 mg/ml protein in 0.4 M $(NH_4)_2SO_4$ and 0.08 M Li_2SO_4 at 10 °C.

X-ray diffraction data were collected at BL 14.1 (HZB, BESSY, Berlin) [58]. The obtained data were processed in space group $P3_212$ using XDS [59] and scaled to a final resolution of 2.0 Å. The phase problem was solved by molecular replacement using the program PHASER [60] with the atomic coordinates of yeast $eIF5_{241-396}$ (PDB 2FUL) as search model. The initial structural model comprised two $eIF5_{241-396}$ molecules per asymmetric unit. Missing regions of the eIF5 construct (residues 201-240) and eIF2β were built manually in Coot [61]. The final model was obtained gradually by iterative rounds of refinement in PHENIX [62], followed by manual model building.

Nuclear Magnetic Resonance (NMR)

NMR experiments were performed in buffer containing 10 mM Na Phosphate, pH 7.0, 150 mM KCl, 1 mM EDTA, 0.02% NaN_3, 1 mM DTT and 0.1 mM AEBSF, with 5% ^2H_2O. NMR data were collected on a 500 MHz Bruker spectrometer (Boston University School of Medicine) equipped with a cryoprobe. NMR resonance assignments for eIF5-CTD were available.[34]

NMR Chemical Shift Perturbation (CSP) assay

The CSP assay was performed using Heteronuclear single-quantum coherence (HSQC) experiments on ^{15}N-labeled proteins. ^{15}N Transverse relaxation optimized spectroscopy (TROSY) HSQC experiments were run on $^{15}N/^2H$-labeled proteins. Chemical shift changes were calculated according to the formula $\delta = ((\delta_H)^2 + (\delta_N/5)^2)^{1/2}$ and affected residues were mapped on the surface of eIF5-CTD, for which the backbone NMR resonance assignments were available.[34] For statistical analysis, average chemical shift changes and standard deviations were calculated in Excel. For K_D determination, $^{15}N/^2H$-labeled or ^{15}N-labeled protein samples were titrated with increasing concentrations of an unlabeled binding partner, until saturation or until solubility limit was reached. Data analysis was done in SigmaPlot, as described previously.[34]

k_{off} estimation from NMR data was based on its effect on exchange broadening (reviewed in [40]). In **Figure 3A**, peaks that move by up to 50 Hz (0.1 ppm for ^{1}H on a 500 MHz NMR spectrometer) are in fast exchange (where peaks move from their position in the free labeled protein to their position in the complex with the ligand as a function of the fraction of bound protein), with no significant exchange broadening. Peaks that move by > 100 Hz (0.2 ppm for ^{1}H) undergo exchange broadening, sometimes beyond detection, at ligand concentrations where a fraction of the protein is bound. Under fast exchange conditions, the line broadening δv, due to exchange is dependent on the chemical shift change between the free and bound state, Δ [s^{-1}]. At equal populations of free and bound states, δv is approximately equal to $(\pi\Delta^2)/4k_{off}$. Therefore, under the experimental conditions (150 mM KCl and 25˚C), if exchange broadening becomes significant for $\Delta > 100\ s^{-1}$, k_{off} is in the order of 100 s^{-1}.

Sequence and structure analysis

Protein BLAST (http://blast.ncbi.nlm.nih.gov/Blast.cgi) was used to obtain initial sequence alignment between human and S. cerevisiae eIF2β. Aligning all six K-boxes was done using Clustal O from the Max-Planck Institute for Developmental Biology Bioinformatics Toolkit (http://toolkit.tuebingen.mpg.de/), followed by manual editing. Instead of by conservation, the aminoacids were colored by hydrophobicity (green), negative charge (red), and positive charge (blue). MOLMOL[63] was used to align the structures of human and S. cerevisiae eIF5-CTD, and for structure visualization.

Data Availability

The atomic model generated in this study will be deposited in the protein data bank prior to publication. The data that support this study are available from corresponding authors upon reasonable request.

Acknowledgments

This work was supported by the National Institute of Health [GM134113 to A.M.].

Author Contributions

Conceptualization, B.K, R.F., and A.M.; Methodology, B.K, R.F., and A.M.; Investigation, P.A.W., M.S., B.K., R.F., and A.M.; Writing – Original Draft, P.A.W., B.K., R.F., and A.M.; Writing – Review & Editing, P.A.W., B.K., R.F., and A.M.; Funding Acquisition, B.K, R.F., and A.M.; Supervision, B.K, R.F., and A.M.

Declaration of interests

The authors declare no competing interests.

Supplemental information

Document S1. Figures S1–S4.

Tables

Table 1. Data collection and refinement statistics for the structure of the eIF5(201-405)·eIF2β(39-106) complex from *S. cerevisiae*

Crystallization	
Condition	0.8 M $(NH_4)SO_4$, 0.3 M $LiSO_4$
Temperature (°C)	20
Data Collection	
Space Group	$P3_212$
Unit Cell	a = 74.3 Å
	b = 74.3 Å
	c = 124.8 Å
	α = 90°
	β = 90°
	γ = 120°
Resolution (Å)	2.0 (2.1-2.0)
Observed reflections	359597 (87743)
Unique reflections	48223 (11831)
Completeness (%)	99.9 (99.8)
$\langle I \rangle/\sigma$	22.3 (3.9)
R_{sym} (%)	8.9 (42.8)
Refinement	
R_{work}/R_{free} (%)	17.4/20.1
Rmsd from Strd. Stereochemistry	
Bond length (Å)	0.007
Bond angles (°)	0.98
Ramachandran Plot Statistics	
Most favored (%)	98.5
Allowed regions (%)	1.5
Disallowed regions (%)	0

Values in parentheses refer to the highest resolution shell.
R_{work} and R_{free} factors are calculated using the formula $R = \Sigma_{hkl}||F(obs)_{hkl}| - |F(calc)_{hkl}||/\Sigma_{hkl}|F(obs)_{hkl}|$, where $F(obs)_{hkl}$ and $F(calc)_{hkl}$ are observed and measured structure factors, respectively. R_{work} and R_{free} differ in the set of reflections they are calculated from: R_{free} is calculated for the test set, whereas R_{work} is calculated for the working set.

Table 2. Binding affinities of WT and phosphomimetic eIF5, eIF2Bε, and 5MP1 for the eIF2β K-boxes

	K_D [μM]			
	K1	**K2**	**K3**	**K123**
eIF5-CTD	3 ± 1	6 ± 1	4 ± 1	(3x) 37 ± 6[1]
eIF2Bε-CTD	8 ± 1	9 ± 3	24 ± 3	(3x) 44 ± 3
5MP1-CTD	20 ± 7	18 ± 3	37 ± 5	(3x) 63 ± 5
eIF5-CTD_EE	0.2 ± 0.2[2]	0.7 ± 0.2[2]	0.3 ± 0.3[2]	(3x) 2.3 ± 0.5
eIF2Bε-CTD_EE	4 ± 1	2.3 ± 0.5	14 ± 1	(3x) 14 ± 4
5MP1-CTD_EE	11 ± 3	5.6 ± 0.9	23 ± 3	(3x) 45 ± 6

[1] The K_Ds for K123 are averages, assuming three binding sites with identical affinities.

[2] K_D values below 1 μM are only approximate because the concentration of the labeled protein (20-50 μM) becomes much larger than the K_D, making accurate fitting difficult.

Figure legends

Figure 1. Crystal Structure of the S. cerevisiae eIF5-CTD:eIF2β-K23 complex.

(A) Crystal structure of the complex between eIF5-CTD (blue) and eIF2β-K23 (yellow). Residues 39-65 of eIF2β, including K2, are not resolved in the electron density, and are therefore not included in the model. The second eIF5-CTD molecule in the asymmetric unit is not shown.

(B) View of the eIF5-CTD:eIF2β-K23 complex centered on the loop containing K3. The eIF5-CTD is shown in surface representation with electrostatic surface charge distribution.

(C) Details of the interaction interface between the αN helix of eIF2β-K3 and the surface of eIF5-CTD.

(D) Details of the interactions of the αC helix of eIF2β-K3 with eIF5-CTD.

(E) Details of the interactions of the K3-loop of eIF2β with eIF5-CTD.

See also Figure S1.

Figure 2. eIF5-CTD forms similar complexes with each of the three K-boxes of eIF2β.

(A) Sequence alignment of the K-boxes and surrounding sequences in *S. cerevisiae* and human eIF2β-NTT, (labeled “Sc 2β” and “Hs 2β”, respectively). The entire 2β-NTT sequences are shown, up to the start of the eIF2γ-binding helix. Residue numbers are shown at the beginning and end of each line. Positively charged amino acids are colored in blue; negatively charged amino acids are colored in red, and hydrophobic amino acids are colored in green. Helices αN and αC from the *S. cerevisiae* eIF5-CTD•eIF2β-K3 complex (**Fig. 1**) are bold and underlined. The corresponding sequence segments in the other K-boxes in *S. cerevisiae* and human eIF2β are underlined. Note that if the K1 and K2 in *S. cerevisiae* form helices of the same length as those observed for K3 (**Fig. 1**), then there are no linker amino acids between K1 and K2, and between K2 and K3 in *S. cerevisiae* eIF2β.

(B) Constructs used in this work. Folded domains are shown as boxes. Intrinsically disordered segments are shown as lines. K-boxes K1, K2, and K3 are marked and colored dark blue, blue, and light blue, respectively. The K3 segment of *S. cerevisiae* eIF2β visible in the crystal structure, including the αN and αC helices (**Fig. 1**) is marked with a solid line. The corresponding segments surrounding the other K-boxes, corresponding to the αN and αC helices are marked with dashed lines. The four point mutations in the putative αN helix are shown with red “X”. eIF2β-NTT is blue. The eIF2γ-binding helix is orange. The homologous C-terminal HEAT (W2) domains of eIF5, eIF2Bε, and 5MP1 are orange. The DWEAR motif in eIF5 is labeled with “DW”.

(C) NMR spectra overlay of $^{15}N/^{2}H$-labeled human eIF5-CTD, free (black) and in the presence of K123 (red), K1 (blue), K2 (green), and K3 (orange). Examples of peaks that are in similar positions or different positions in the different complexes are boxed.

(D) Comparison of eIF2β K-box contacts in yeast and human, in cross-eyed stereo. The eIF2β-K3 segment from the crystal structure of the *S. cerevisiae* eIF5-CTD•eIF2β-K3 complex (**Fig. 1**) is overlayed on the structure of human eIF5-CTD (2iu1.pdb[39]). The overlay was obtained by

aligning the structures of human and yeast eIF5-CTD. eIF2β is shown as a blue ribbon, with sidechains also shown. Human eIF5-CTD is shown in surface representation colored by CSP effects for K123 binding: from dark orange (large effects) to yellow (small effects). No significant changes are light grey; amino-acids that could not be analyzed are in dark grey. eIF5-CTT is disordered in solution[34] and shown as a ribbon.

See also Figures S2 and S3.

Figure 3. Binding affinities of eIF5-CTD, eIF2Bε-CTD, and 5MP1-CTD for eIF2β-NTT and its individual K-boxes.

(A) NMR spectra overlay of titration of $^{15}N/^{2}H$-labeled 5-CTD with K1, with insets for a couple of moving peaks in fast and intermediate exchange.

(B) Overlay of titration curves of eIF5-CTD binding to K1, K2, K3, and K123. The calculated K_Ds and standard errors (SE) are shown in the inset.

(C) Overlay of titration curves of eIF2Bε-CTD binding to K1, K2, K3, and K123.

(D) Overlay of titration curves of 5MP1-CTD binding to K1, K2, K3, and K123. Note that the K_Ds for K123 are averages, assuming three binding sites with identical affinities.

Figure 4. Binding affinities of eIF5-CTD-EE, eIF2Bε-CTD-EE, and 5MP1-CTD-EE for eIF2β-NTT and its individual K-boxes.

(A) Overlay of titration curves of eIF5-CTD-EE binding to K1, K2, K3, and K123. The calculated K_Ds and standard errors (SE) are shown in the inset.

(B) Overlay of titration curves of eIF2Bε-CTD-EE binding to K1, K2, K3, and K123.

(C) Overlay of titration curves of 5MP1-CTD-EE binding to K1, K2, K3, and K123. Note that the K_Ds for K123 are averages, assuming three binding sites with identical affinities.

Figure 5. Model for the handoff of eIF2 between eIF5 and eIF2B.

Folded domains are shown as shapes. Intrinsically disordered regions are shown as lines. eIF2 is yellow; eIF5 is brown; eIF2B is blue. The shapes of the folded segments of eIF2 and eIF2B, their mutual orientations, and contacts are based on the eIF2B•eIF2 complex structure (6jlw.pdb[24]). For simplicity, only one eIF2 is shown bound to eIF2B. Interactions are shown with double arrows, instead of with physical contacts in the complex, to emphasize their dynamic nature. The mutual destabilization between two proteins simultaneously bound to eIF2β-NTT is illustrated by red T-shaped lines. The same mechanism could work in the opposite direction in the handoff of the TC from eIF2B to eIF5, except there eIF2α-NTD would be interaction with the Met-tRNAi, instead of with eIF2B.

References

1 Brito Querido, J., Diaz-Lopez, I., and Ramakrishnan, V. (2024). The molecular basis of translation initiation and its regulation in eukaryotes. Nat Rev Mol Cell Biol *25*, 168-186.
2 Dever, T.E., Ivanov, I.P., and Hinnebusch, A.G. (2023). Translational regulation by uORFs and start codon selection stringency. Genes & development *37*, 474-489.
3 Jackson, R.J., Hellen, C.U., and Pestova, T.V. (2010). The mechanism of eukaryotic translation initiation and principles of its regulation. Nat Rev Mol Cell Biol *11*, 113-127.
4 Marintchev, A., and Wagner, G. (2004). Translation initiation: structures, mechanisms and evolution. Q Rev Biophys *37*, 197-284.
5 Weisser, M., and Ban, N. (2019). Extensions, Extra Factors, and Extreme Complexity: Ribosomal Structures Provide Insights into Eukaryotic Translation. Cold Spring Harb Perspect Biol *11*.
6 Jennings, M.D., and Pavitt, G.D. (2010). eIF5 has GDI activity necessary for translational control by eIF2 phosphorylation. Nature *465*, 378-381.
7 Jennings, M.D., Zhou, Y., Mohammad-Qureshi, S.S., Bennett, D., and Pavitt, G.D. (2013). eIF2B promotes eIF5 dissociation from eIF2*GDP to facilitate guanine nucleotide exchange for translation initiation. Genes & development *27*, 2696-2707.
8 Singh, C.R., Lee, B., Udagawa, T., Mohammad-Qureshi, S.S., Yamamoto, Y., Pavitt, G.D., and Asano, K. (2006). An eIF5/eIF2 complex antagonizes guanine nucleotide exchange by eIF2B during translation initiation. The EMBO journal *25*, 4537-4546.
9 Bogorad, A.M., Lin, K.Y., and Marintchev, A. (2018). eIF2B Mechanisms of Action and Regulation: A Thermodynamic View. Biochemistry *57*, 1426-1435.
10 Hinnebusch, A.G. (2014). The scanning mechanism of eukaryotic translation initiation. Annu Rev Biochem *83*, 779-812.
11 Marintchev, A., and Ito, T. (2020). eIF2B and the Integrated Stress Response: A Structural and Mechanistic View. Biochemistry *59*, 1299-1308.
12 Dever, T.E., Dar, A.C., and Sicheri, F. (2007). The eIF2α kinases. In Translational Control in Biology and Medicine, M.B. Mathews, Sonenberg, N., Hershey, J. W. B., ed. (Cold Spring harbor, NY: Cold Spring Harbor Laboratory Press), pp. 319-344.
13 Hinnebusch, A.G. (2005). Translational regulation of GCN4 and the general amino acid control of yeast. Annu Rev Microbiol *59*, 407-450.
14 Hinnebusch, A.G., Dever, T.E., and Asano, K. (2007). Mechanism of translation initiation in the yeast *Saccharomyces cerevisiae.* In Translational Control in Biology and Medicine, M.B. Mathews, Sonenberg, N., Hershey, J. W. B., ed. (Cold Spring harbor, NY: Cold Spring Harbor Laboratory Press), pp. 225-268.
15 Ron, D., and Harding, H.P. (2007). eIF2α phosphorylation in cellular stress responses and disease. In Translational Control in Biology and Medicine, M.B. Mathews, Sonenberg, N., Hershey, J. W. B., ed. (Cold Spring harbor, NY: Cold Spring Harbor Laboratory Press), pp. 345-368.
16 Wek, R.C., Jiang, H.Y., and Anthony, T.G. (2006). Coping with stress: eIF2 kinases and translational control. Biochem Soc Trans *34*, 7-11.
17 Kozel, C., Thompson, B., Hustak, S., Moore, C., Nakashima, A., Singh, C.R., Reid, M., Cox, C., Papadopoulos, E., Luna, R.E.*, et al.* (2016). Overexpression of eIF5 or its protein mimic 5MP perturbs eIF2 function and induces ATF4 translation through delayed re-initiation. Nucleic acids research *44*, 8704-8713.
18 Singh, C.R., Glineburg, M.R., Moore, C., Tani, N., Jaiswal, R., Zou, Y., Aube, E., Gillaspie, S., Thornton, M., Cecil, A.*, et al.* (2021). Human oncoprotein 5MP suppresses general and repeat-associated non-AUG translation via eIF3 by a common mechanism. Cell Rep *36*, 109376.

19 Tang, L., Morris, J., Wan, J., Moore, C., Fujita, Y., Gillaspie, S., Aube, E., Nanda, J., Marques, M., Jangal, M.*, et al.* (2017). Competition between translation initiation factor eIF5 and its mimic protein 5MP determines non-AUG initiation rate genome-wide. Nucleic acids research *45*, 11941-11953.
20 Luna, R.E., Arthanari, H., Hiraishi, H., Akabayov, B., Tang, L., Cox, C., Markus, M.A., Luna, L.E., Ikeda, Y., Watanabe, R.*, et al.* (2013). The interaction between eukaryotic initiation factor 1A and eIF5 retains eIF1 within scanning preinitiation complexes. Biochemistry *52*, 9510-9518.
21 Luna, R.E., Arthanari, H., Hiraishi, H., Nanda, J., Martin-Marcos, P., Markus, M.A., Akabayov, B., Milbradt, A.G., Luna, L.E., Seo, H.C.*, et al.* (2012). The C-terminal domain of eukaryotic initiation factor 5 promotes start codon recognition by its dynamic interplay with eIF1 and eIF2beta. Cell Rep *1*, 689-702.
22 Obayashi, E., Luna, R.E., Nagata, T., Martin-Marcos, P., Hiraishi, H., Singh, C.R., Erzberger, J.P., Zhang, F., Arthanari, H., Morris, J.*, et al.* (2017). Molecular Landscape of the Ribosome Pre-initiation Complex during mRNA Scanning: Structural Role for eIF3c and Its Control by eIF5. Cell Rep *18*, 2651-2663.
23 Alone, P.V., and Dever, T.E. (2006). Direct binding of translation initiation factor eIF2gamma-G domain to its GTPase-activating and GDP-GTP exchange factors eIF5 and eIF2B epsilon. The Journal of biological chemistry *281*, 12636-12644.
24 Kashiwagi, K., Yokoyama, T., Nishimoto, M., Takahashi, M., Sakamoto, A., Yonemochi, M., Shirouzu, M., and Ito, T. (2019). Structural basis for eIF2B inhibition in integrated stress response. Science *364*, 495-499.
25 Kenner, L.R., Anand, A.A., Nguyen, H.C., Myasnikov, A.G., Klose, C.J., McGeever, L.A., Tsai, J.C., Miller-Vedam, L.E., Walter, P., and Frost, A. (2019). eIF2B-catalyzed nucleotide exchange and phosphoregulation by the integrated stress response. Science *364*, 491-495.
26 Homma, M.K., Wada, I., Suzuki, T., Yamaki, J., Krebs, E.G., and Homma, Y. (2005). CK2 phosphorylation of eukaryotic translation initiation factor 5 potentiates cell cycle progression. Proceedings of the National Academy of Sciences of the United States of America *102*, 15688-15693.
27 Singh, L.P., Denslow, N.D., and Wahba, A.J. (1996). The interaction of rabbit reticulocyte guanine nucleotide exchange factor eIF-2B with chain initiation factor 2: studies with N-ethylmaleimide and trypsin. Biochem Biophys Res Commun *223*, 604-611.
28 Borgo, C., Franchin, C., Scalco, S., Bosello-Travain, V., Donella-Deana, A., Arrigoni, G., Salvi, M., and Pinna, L.A. (2017). Generation and quantitative proteomics analysis of CK2alpha/alpha'((-/-)) cells. Sci Rep *7*, 42409.
29 Franchin, C., Borgo, C., Cesaro, L., Zaramella, S., Vilardell, J., Salvi, M., Arrigoni, G., and Pinna, L.A. (2018). Re-evaluation of protein kinase CK2 pleiotropy: new insights provided by a phosphoproteomics analysis of CK2 knockout cells. Cell Mol Life Sci *75*, 2011-2026.
30 Gandin, V., Masvidal, L., Cargnello, M., Gyenis, L., McLaughlan, S., Cai, Y., Tenkerian, C., Morita, M., Balanathan, P., Jean-Jean, O.*, et al.* (2016). mTORC1 and CK2 coordinate ternary and eIF4F complex assembly. Nat Commun *7*, 11127.
31 Llorens, F., Roher, N., Miro, F.A., Sarno, S., Ruiz, F.X., Meggio, F., Plana, M., Pinna, L.A., and Itarte, E. (2003). Eukaryotic translation-initiation factor eIF2beta binds to protein kinase CK2: effects on CK2alpha activity. Biochem J *375*, 623-631.
32 Paytubi, S., Morrice, N.A., Boudeau, J., and Proud, C.G. (2008). The N-terminal region of ABC50 interacts with eukaryotic initiation factor eIF2 and is a target for regulatory phosphorylation by CK2. Biochem J *409*, 223-231.
33 Turowec, J.P., Duncan, J.S., French, A.C., Gyenis, L., St Denis, N.A., Vilk, G., and Litchfield, D.W. (2010). Protein kinase CK2 is a constitutively active enzyme that promotes cell survival: strategies to identify CK2 substrates and manipulate its activity in mammalian cells. Methods in enzymology *484*, 471-493.

34 Paul, E.E., Lin, K.Y., Gamble, N., Tsai, A.W., Swan, S.H.K., Yang, Y., Doran, M., and Marintchev, A. (2022). Dynamic interaction network involving the conserved intrinsically disordered regions in human eIF5. Biophys Chem *281*, 106740.
35 Gamble, N., Paul, E.E., Anand, B., and Marintchev, A. (2022). Regulation of the interactions between human eIF5 and eIF1A by the CK2 kinase. Curr Res Struct Biol *4*, 308-319.
36 Wei, Z., Xue, Y., Xu, H., and Gong, W. (2006). Crystal structure of the C-terminal domain of S.cerevisiae eIF5. J Mol Biol *359*, 1-9.
37 Das, S., and Maitra, U. (2000). Mutational analysis of mammalian translation initiation factor 5 (eIF5): role of interaction between the beta subunit of eIF2 and eIF5 in eIF5 function in vitro and in vivo. Mol Cell Biol *20*, 3942-3950.
38 Yamamoto, Y., Singh, C.R., Marintchev, A., Hall, N.S., Hannig, E.M., Wagner, G., and Asano, K. (2005). The eukaryotic initiation factor (eIF) 5 HEAT domain mediates multifactor assembly and scanning with distinct interfaces to eIF1, eIF2, eIF3, and eIF4G. Proceedings of the National Academy of Sciences of the United States of America *102*, 16164-16169.
39 Bieniossek, C., Schutz, P., Bumann, M., Limacher, A., Uson, I., and Baumann, U. (2006). The crystal structure of the carboxy-terminal domain of human translation initiation factor eIF5. J Mol Biol *360*, 457-465.
40 Marintchev, A., Frueh, D., and Wagner, G. (2007). NMR methods for studying protein-protein interactions involved in translation initiation. Methods in enzymology *430*, 283-331.
41 Mertins, P., Mani, D.R., Ruggles, K.V., Gillette, M.A., Clauser, K.R., Wang, P., Wang, X., Qiao, J.W., Cao, S., Petralia, F.*, et al.* (2016). Proteogenomics connects somatic mutations to signalling in breast cancer. Nature *534*, 55-62.
42 Yi, T., Zhai, B., Yu, Y., Kiyotsugu, Y., Raschle, T., Etzkorn, M., Seo, H.C., Nagiec, M., Luna, R.E., Reinherz, E.L.*, et al.* (2014). Quantitative phosphoproteomic analysis reveals system-wide signaling pathways downstream of SDF-1/CXCR4 in breast cancer stem cells. Proceedings of the National Academy of Sciences of the United States of America *111*, E2182-2190.
43 Asano, K., Krishnamoorthy, T., Phan, L., Pavitt, G.D., and Hinnebusch, A.G. (1999). Conserved bipartite motifs in yeast eIF5 and eIF2Bepsilon, GTPase-activating and GDP-GTP exchange factors in translation initiation, mediate binding to their common substrate eIF2. The EMBO journal *18*, 1673-1688.
44 Hiraishi, H., Oatman, J., Haller, S.L., Blunk, L., McGivern, B., Morris, J., Papadopoulos, E., Gutierrez, W., Gordon, M., Bokhari, W.*, et al.* (2014). Essential role of eIF5-mimic protein in animal development is linked to control of ATF4 expression. Nucleic acids research *42*, 10321-10330.
45 Huang, Q., Szklarczyk, D., Wang, M., Simonovic, M., and von Mering, C. (2023). PaxDb 5.0: Curated Protein Quantification Data Suggests Adaptive Proteome Changes in Yeasts. Mol Cell Proteomics *22*, 100640.
46 Dokladal, L., Stumpe, M., Pillet, B., Hu, Z., Garcia Osuna, G.M., Kressler, D., Dengjel, J., and De Virgilio, C. (2021). Global phosphoproteomics pinpoints uncharted Gcn2-mediated mechanisms of translational control. Molecular cell *81*, 1879-1889 e1876.
47 Panniers, R., and Henshaw, E.C. (1983). A GDP/GTP exchange factor essential for eukaryotic initiation factor 2 cycling in Ehrlich ascites tumor cells and its regulation by eukaryotic initiation factor 2 phosphorylation. The Journal of biological chemistry *258*, 7928-7934.
48 Gross, M., Rubino, M.S., and Hessefort, S.M. (1991). The conversion of eIF-2.GDP to eIF-2.GTP by eIF-2B requires Met-tRNA(fMet). Biochem Biophys Res Commun *181*, 1500-1507.
49 Siekierka, J., Mitsui, K.I., and Ochoa, S. (1981). Mode of action of the heme-controlled translational inhibitor: relationship of eukaryotic initiation factor 2-stimulating protein to

translation restoring factor. Proceedings of the National Academy of Sciences of the United States of America *78*, 220-223.
50 Loughran, G., Firth, A.E., Atkins, J.F., and Ivanov, I.P. (2018). Translational autoregulation of BZW1 and BZW2 expression by modulating the stringency of start codon selection. PLoS One *13*, e0192648.
51 Borgo, C., D'Amore, C., Cesaro, L., Itami, K., Hirota, T., Salvi, M., and Pinna, L.A. (2020). A N-terminally deleted form of the CK2alpha' catalytic subunit is sufficient to support cell viability. Biochem Biophys Res Commun *531*, 409-415.
52 Mukhopadhyay, S., Amodeo, M.E., and Lee, A.S.Y. (2023). eIF3d controls the persistent integrated stress response. Molecular cell *83*, 3303-3313 e3306.
53 Lamper, A.M., Fleming, R.H., Ladd, K.M., and Lee, A.S.Y. (2020). A phosphorylation-regulated eIF3d translation switch mediates cellular adaptation to metabolic stress. Science *370*, 853-856.
54 Lee, A.S., Kranzusch, P.J., Doudna, J.A., and Cate, J.H. (2016). eIF3d is an mRNA cap-binding protein that is required for specialized translation initiation. Nature *536*, 96-99.
55 Loughran, G., Sachs, M.S., Atkins, J.F., and Ivanov, I.P. (2012). Stringency of start codon selection modulates autoregulation of translation initiation factor eIF5. Nucleic acids research *40*, 2898-2906.
56 Ivanov, I.P., Loughran, G., Sachs, M.S., and Atkins, J.F. (2010). Initiation context modulates autoregulation of eukaryotic translation initiation factor 1 (eIF1). Proceedings of the National Academy of Sciences of the United States of America *107*, 18056-18060.
57 Milo, R., Jorgensen, P., Moran, U., Weber, G., and Springer, M. (2010). BioNumbers--the database of key numbers in molecular and cell biology. Nucleic acids research *38*, D750-753.
58 Mueller, U., Darowski, N., Fuchs, M.R., Forster, R., Hellmig, M., Paithankar, K.S., Puhringer, S., Steffien, M., Zocher, G., and Weiss, M.S. (2012). Facilities for macromolecular crystallography at the Helmholtz-Zentrum Berlin. J Synchrotron Radiat *19*, 442-449.
59 Kabsch, W. (2010). Integration, scaling, space-group assignment and post-refinement. Acta Crystallogr D Biol Crystallogr *66*, 133-144.
60 McCoy, A.J., Grosse-Kunstleve, R.W., Adams, P.D., Winn, M.D., Storoni, L.C., and Read, R.J. (2007). Phaser crystallographic software. J Appl Crystallogr *40*, 658-674.
61 Emsley, P., Lohkamp, B., Scott, W.G., and Cowtan, K. (2010). Features and development of Coot. Acta Crystallogr D Biol Crystallogr *66*, 486-501.
62 Adams, P.D., Afonine, P.V., Bunkoczi, G., Chen, V.B., Davis, I.W., Echols, N., Headd, J.J., Hung, L.W., Kapral, G.J., Grosse-Kunstleve, R.W.*, et al.* (2010). PHENIX: a comprehensive Python-based system for macromolecular structure solution. Acta Crystallogr D Biol Crystallogr *66*, 213-221.
63 Koradi, R., Billeter, M., and Wuthrich, K. (1996). MOLMOL: a program for display and analysis of macromolecular structures. J Mol Graph *14*, 51-55, 29-32.

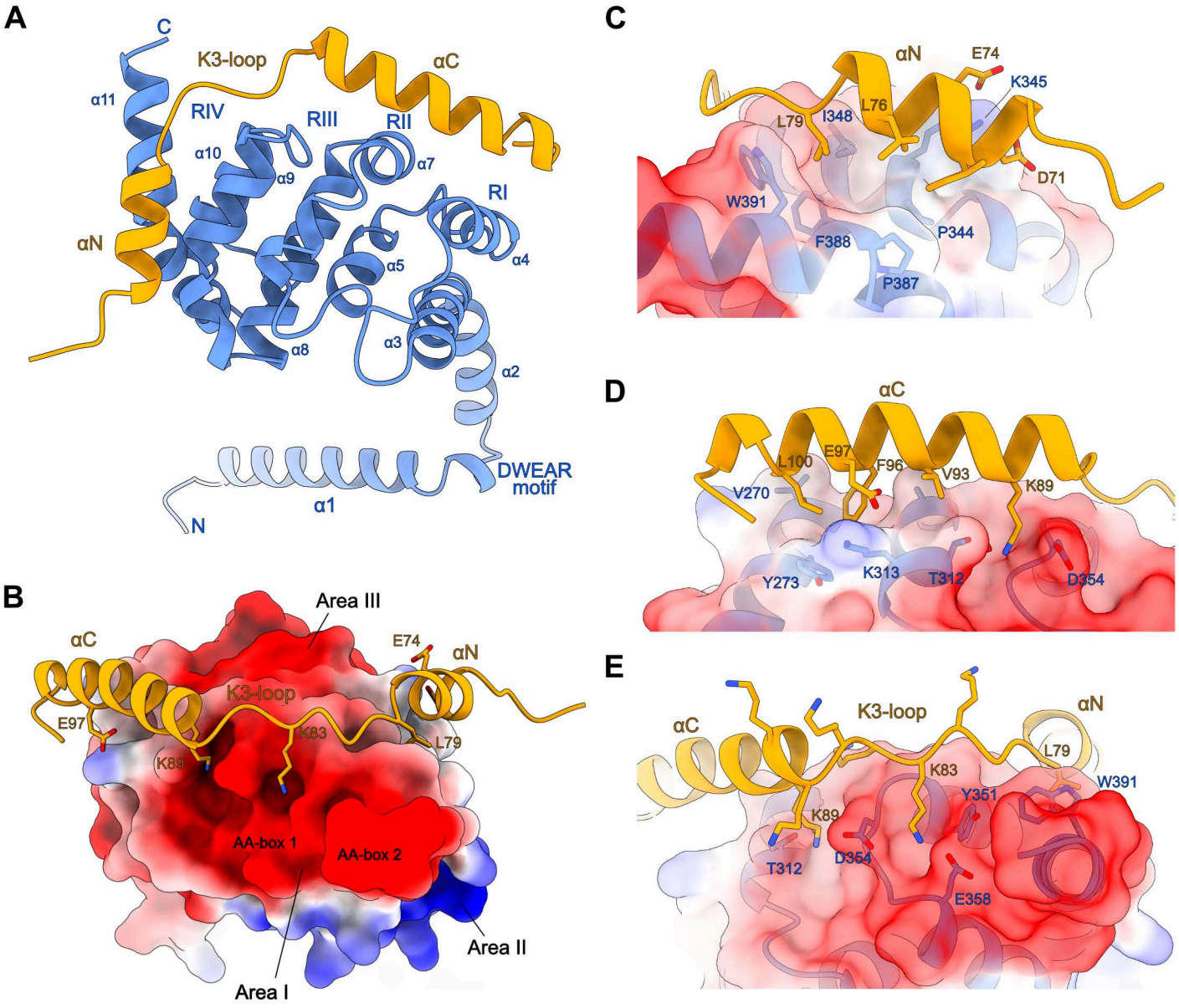
A
C
K3-loop
αC
α11
RIV
RIII
RII
α10
α9
α7
RI
αN
α5
α4
α8
α3
α2
DWEAR
motif
α1
N
B
Area III
αC
E74
αN
K3-loop
E97
K83
L79
K89
AA-box 1
AA-box 2
Area II
Area I
C
αN
E74
K345
L76
L79
I348
D71
W391
P344
F388
P387
D
αC
E97
L100
F96
V93
V270
K89
Y273
K313
T312
D354
E
αC
K3-loop
αN
L79
K83
W391
Y351
K89
T312
D354
E358

A eIF2β K-box sequence alignment

```
Sc 2β 1     MSSDLAAELGFDPALKKKKKTKKVIPDDFDAAVNGK------------------------------  36
Hs 2β 1        MSGDEMIFDPTMSKKKKKKKKPFMLDEEGDTQTEETQPSETKEVEPEPTEDKDLEADEEDTRK  64
Sc 2β 37    ---ENGSGDDLFAGLKKKKKKSKSVSADAEAEKEPT------------------------------  69
Hs 2β 65    KDASDDLDDLNFFNQKKKKKKTKKIFDIDEAEEGVKDLKIESDVQ--------------------- 108
Sc 2β 70    ---DDIAEALGELSLKKKKKKTKDSSVDAFEKELAKAGLDNVDAESKEGTPSANS---SIQQEVGL 129
Hs 2β 109   EPTEPEDDLDIMLGNKKKKKKNVKFPDEDEILEKDEALEDEDNKKDDGISFSNQTGPAWAGSERDY 174
```

B Constructs used in this study

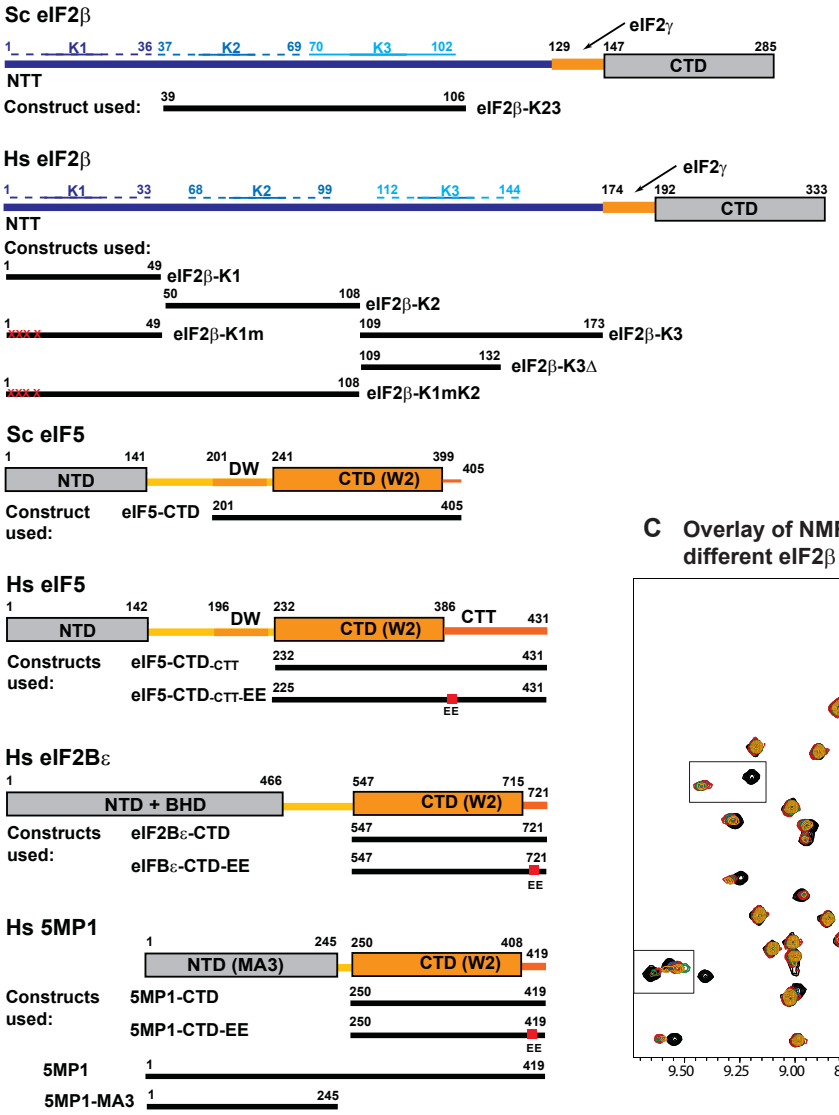

C Overlay of NMR spectra of Hs eIF5-CTD in the absence and presence of different eIF2β K-boxes

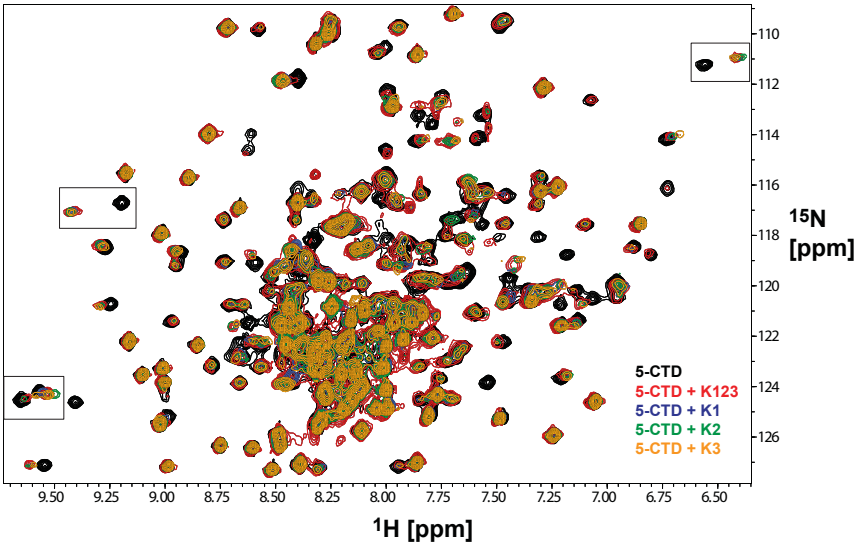

D Comparison of eIF2β K-box contacts in yeast and human

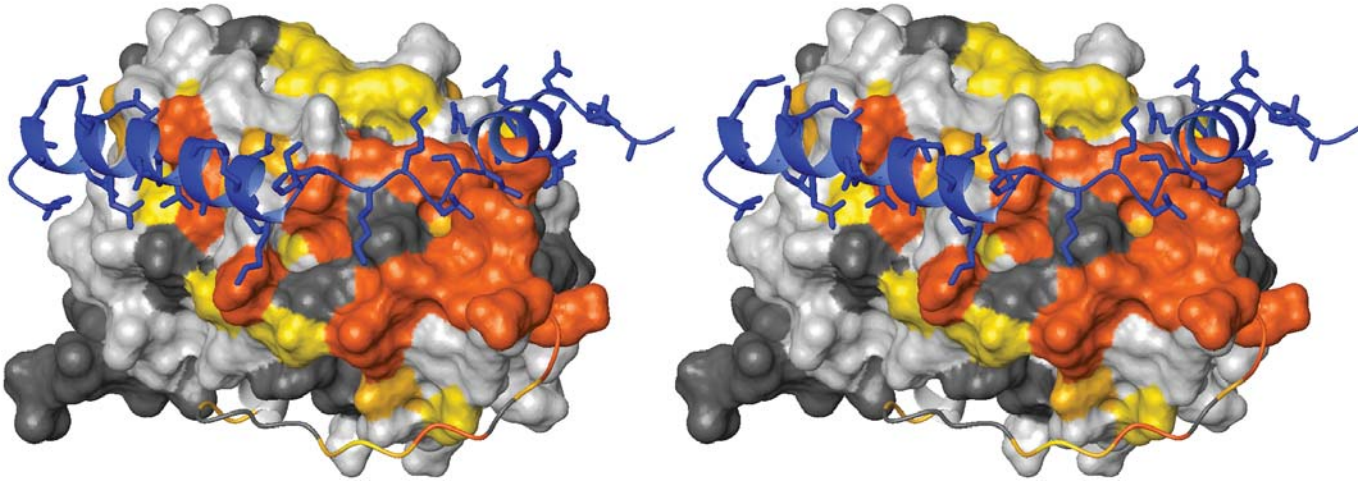

A NMR titration of eIF5-CTD with eIF2β K3

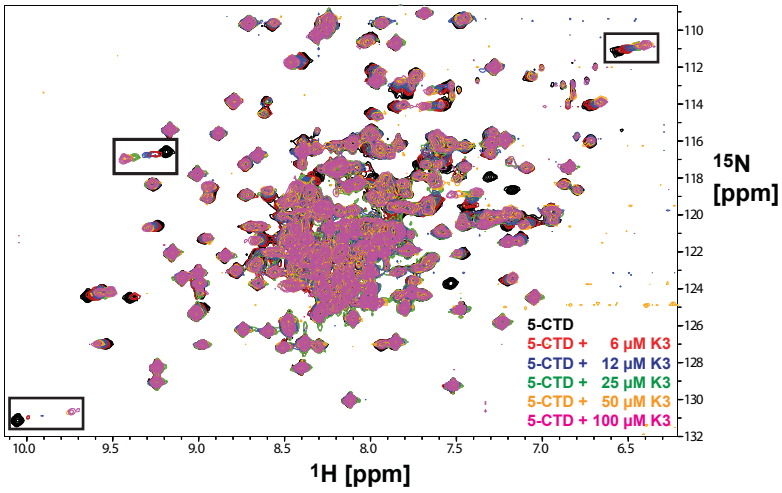

B Affinities of eIF2β constructs for eIF5-CTD

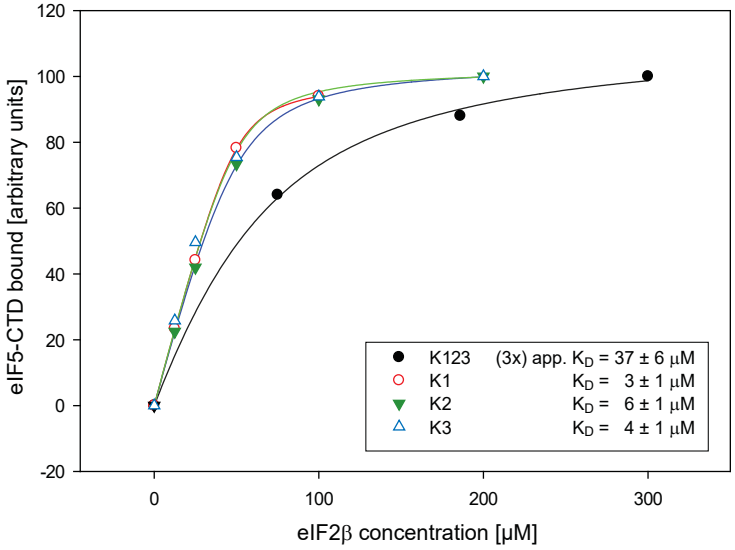

C Affinities of eIF2β constructs for eIF2Bε-CTD

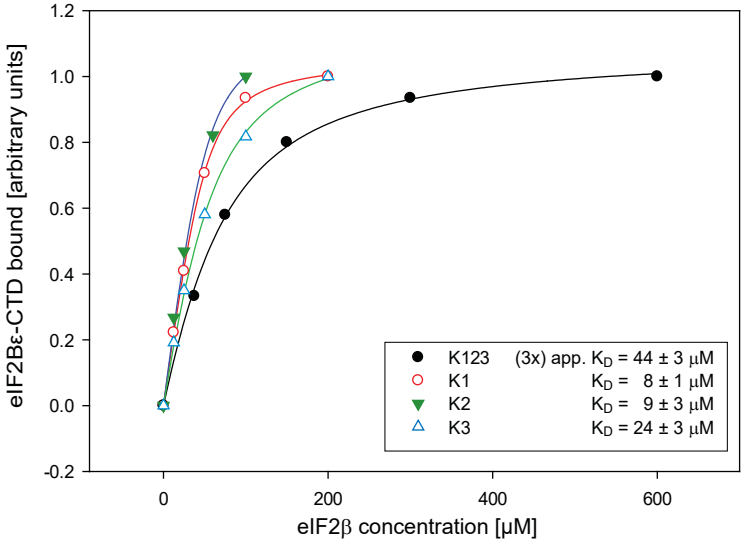

D Affinities of eIF2β constructs for 5MP1-CTD

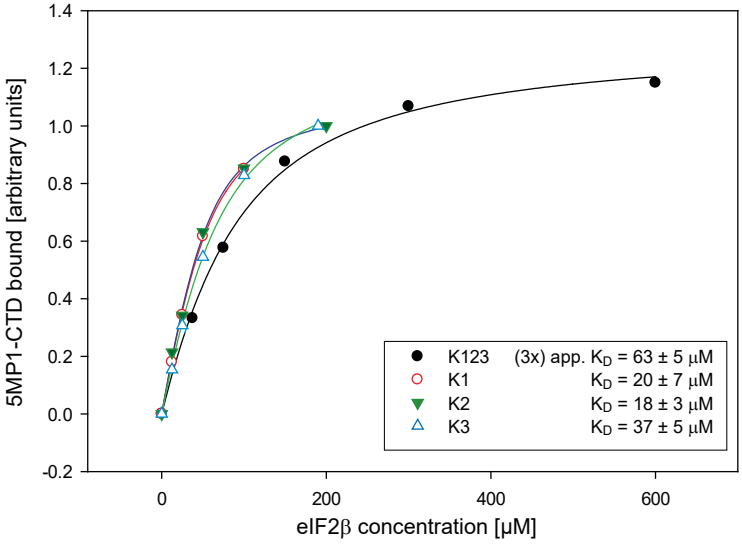

A **Affinities of eIF2β constructs for eIF5-CTD-EE**

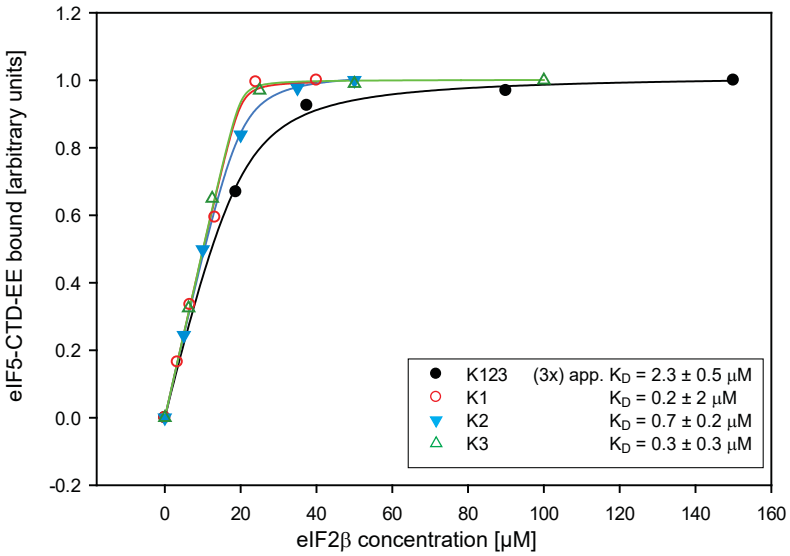

B **Affinities of eIF2β constructs for eIF2Bε-CTD-EE**

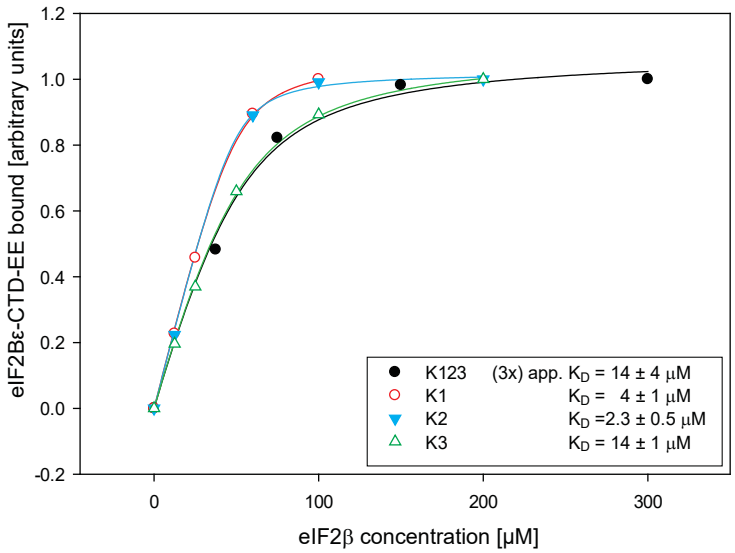

C **Affinities of eIF2β constructs for 5MP1-CTD-EE**

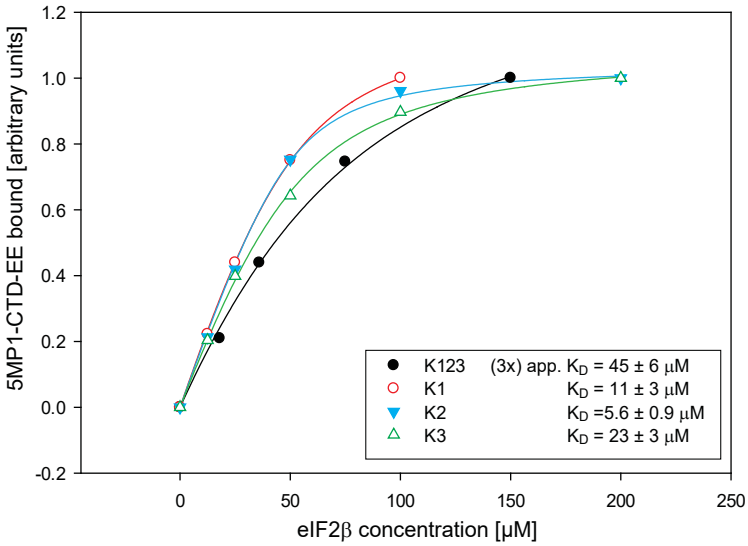

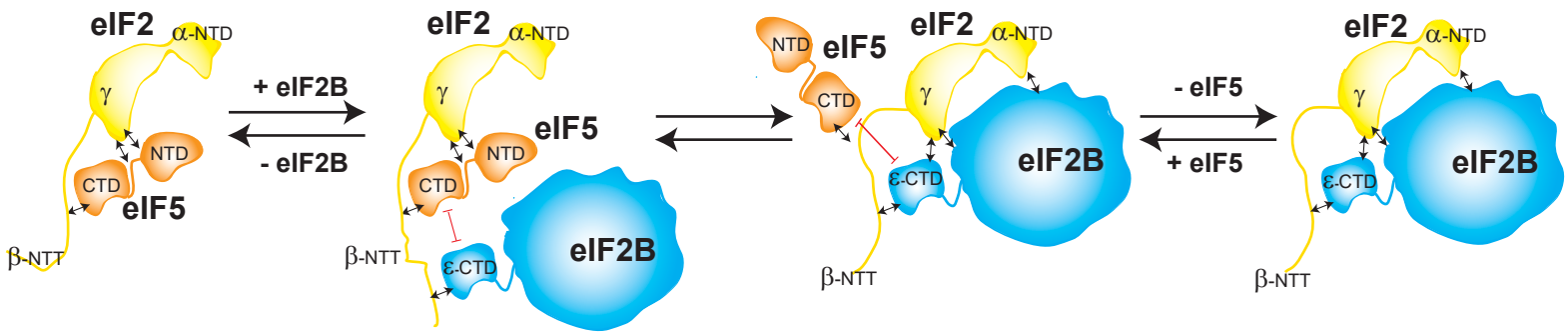
eIF2
α-NTD
γ
NTD
CTD
eIF5
β-NTT
+ eIF2B
- eIF2B
eIF2
α-NTD
γ
NTD
eIF5
CTD
ε-CTD
eIF2B
β-NTT
NTD
eIF5
CTD
eIF2
α-NTD
γ
ε-CTD
eIF2B
β-NTT
- eIF5
+ eIF5
eIF2
α-NTD
γ
ε-CTD
eIF2B
β-NTT